Supporting Information

Effects of helium implantation on the tensile properties and microstructure of $Ni_{73}P_{27}$ metallic glass nanostructures

Rachel Liontas[1], X. Wendy Gu[1], Engang Fu[2], Yongqiang Wang[2], Nan Li[2], Nathan Mara[2], and Julia R. Greer[3,4]*

[1]Division of Chemistry and Chemical Engineering, California Institute of Technology, Pasadena CA, 91125

[2]Los Alamos National Laboratory, Los Alamos, NM 87544

[3]Division of Engineering and Applied Sciences, California Institute of Technology, Pasadena CA, 91125

[4]The Kavli Nanoscience Institute, California Institute of Technology, Pasadena CA, 91125

*Corresponding author

E-mail address: jrgreer@caltech.edu

Sample Fabrication

Samples were fabricated using electron beam lithography and electroplating to create arrays of vertically oriented nano-cylinders, following the methodology of Burek et al.[1]. In this methodology, the nano-cylinder arrays were fabricated on 1 cm^2 Si substrates covered by a 20 nm thick Ti adhesion layer and a 100 nm thick Au seed layer deposited on the substrates by electron beam evaporation. The conductive Au seed layer serves as a cathode in electroplating of the nano-mechanical testing specimens. PMMA 495A8 resist (Micro-Chem Corp.) is spin-coated at 4000 rpm on top of the Si/Ti/Au layers to create a ~500 nm thick layer of PMMA. The PMMA is patterned by electron beam lithography (Leica Electron-Beam-Pattern-Generator 5000+) to create a template of vertical pores, and Ni-P is electroplated into these pores. The electrodeposition occur according to the following cathodic reaction mechanism[2]:

$$Ni^{2+} + 2e^- \rightarrow Ni(s) \quad (1)$$

$$HPO_3^{2-} + 2H_2O + 2e^- \rightarrow H_2PO_2^- + 3OH^- \quad (2)$$

$$H_2PO_2^- + e^- \rightarrow P(s) + 2OH^- \quad (3)$$

During electroplating, a constant current between the anode (Ni foil) and the cathode (Au) is provided, and tensile specimens are formed by electroplating the Ni-P metallic glass above the level of the PMMA surface to create hemispherical-shaped “mushroom caps” on top of the nano-cylinders. After electroplating, the PMMA template is removed by dissolution in acetone, resulting in a free-standing array of vertically oriented Ni-P nano-cylinders with “mushroom caps”. Before tensile testing, the electroplated Ni-P nano-cylinders were secured to the Au substrate by using the electron-beam in an SEM (Nova 200 Nanolab, FEI co.) to deposit a small amount of W at the base of the nano-cylinder. This W deposition was performed at an energy of 30 keV and a current of 0.63 nA.

Helium implantation

Helium implantation was conducted using a Danfysik 200 kV ion implanter at Los Alamos National Laboratory. The samples were mounted with silver paste onto a large Cu holder, which served as a heat sink. The temperature at the Cu mount was continuously measured and kept at room temperature. The energies and fluences were selected according to SRIM calculation to create an overall uniform helium concentration of ~3 at. % throughout each sample. The implantations were performed in order of highest energy to lowest energy: 200 keV, 150 keV, 100 keV, and then 50 keV.

Tensile testing

Several factors can affect the apparent elastic modulus obtained via nano-mechanical testing. Such factors include slight misalignments between tension grips and sample, roughness or imperfections on the sample and tensile grip surfaces, substrate effects, and machine compliance. Consequently, the raw displacement data obtained during testing leads to results with high variability in the elastic modulus, which is an unavoidable characteristic shortcoming of nano-mechanical testing [3-5]. To obtain more accurate results, instead of using the raw data of the measured displacement signal, frames from the in-situ SEM videos were examined to determine the actual displacement. This technique allows for more reliable strain data and has been used successfully in many publications[5-7]. The InSEM system (Nanomechanics, Inc.) used has a load resolution of 3 nN and a displacement resolution of 0.0002 nm. *In-situ* SEM tensile testing also allowed the identification of tests with noticeable bending of the nano-cylinder or tilting of the nano-cylinder "mushroom-cap". These tests were then discarded as unreliable. In addition only tests where fracture occurred in the gauge section of the nano-cylinder were used; tests where the

sample fractured at the Au substrate or at the top of the gauge section near the nano-cylinder's "mushroom cap" were discarded. Such tests where fracture occurred near the very top or bottom of the nano-cylinder had noticeably lower strength, indicating those tests merely tested the strength of adhesion to the substrate or a reduced failure strength due to stress concentrated at the joint between "mushroom cap" and cylinder, and not actual strength of the nano-cylinder gauge section.

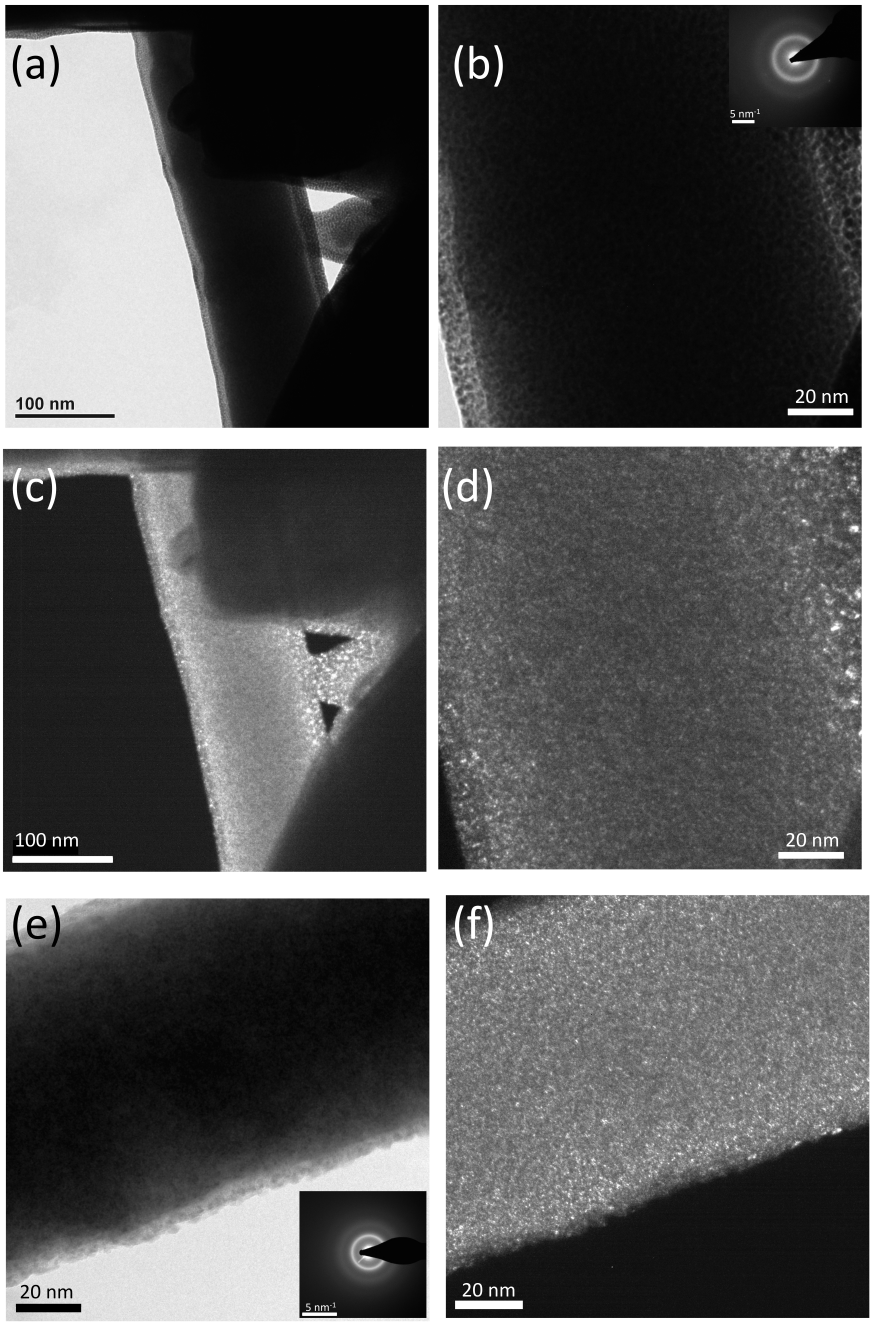

Figure S1. He-implanted nano-cylinder TEM analysis on two individual specimens. The first specimen is shown in **(a)-(d)** and the second specimen is shown in **(e)-(f)**. **(a)** bright field image of entire nano-cylinder (center of image) on Cu TEM grid (right side of image). **(b)** bright field image of zoomed in region near center of nano-cylinder with inset diffraction pattern. **(c)** dark field image of entire nano-cylinder (center of image) on Cu TEM grid (right side of image). **(d)** dark field image of zoomed-in region near center of nano-cylinder. Similar **(e)** bright field and **(f)** dark-field image are provided from another He-implanted specimen for further corroboration. The brighter spots on edges of the specimen in (d) and (f) indicative of crystallites present in the deposited W glue used to secure the specimen to the TEM grid.

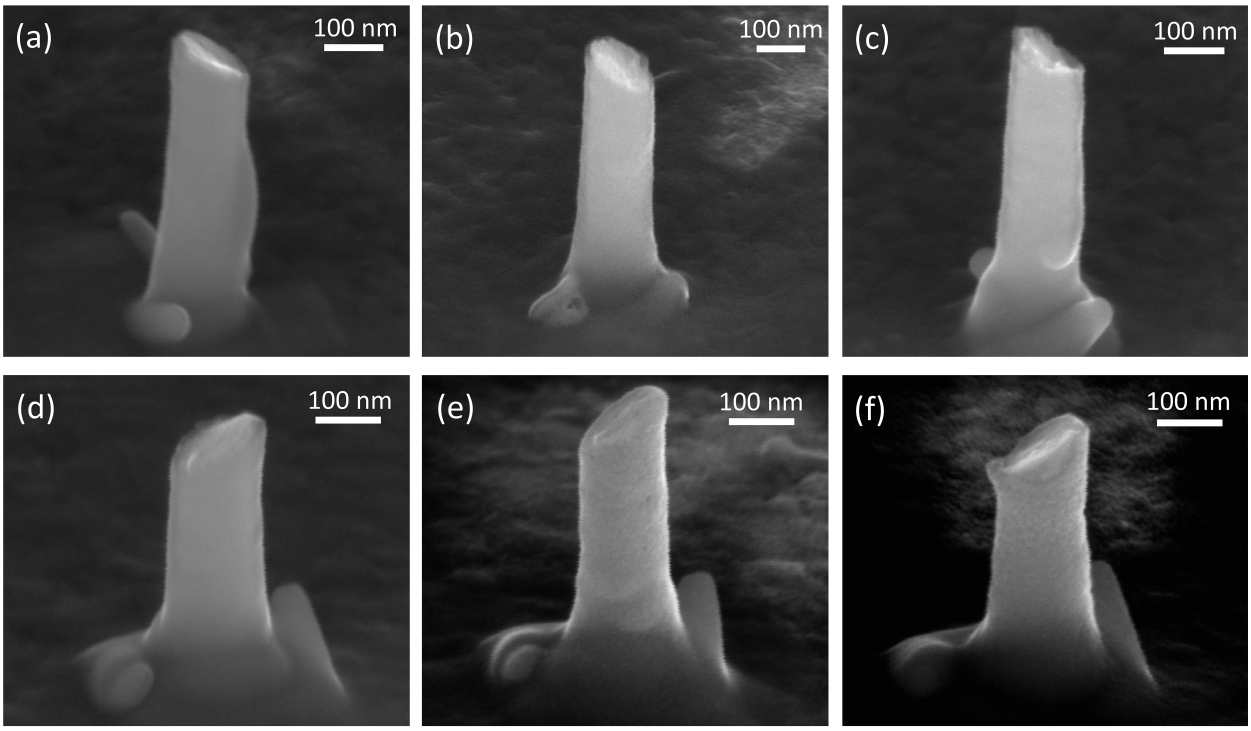

Figure S2. SEM images of the nano-cylinder fracture surfaces after tensile testing for **(a)-(c)** as-fabricated and **(d)-(e)** He-implanted specimens. As noted in the manuscript, all specimens failed at a ~45° angle with respect to the loading axis indicating a similar shear-banding failure mechanism in both as-fabricated and He-implanted specimens.

(1) Burek, M. J. and Greer, J. R. *Nano Lett*. **2010**, *10*, 69–76.
(2) Ng, P. K.; Snyder, D. D.; LaSala, J.; Clemens, B.; and Fuerst, C. *J. Electrochem. Soc*. **1988**, *135*, 1376–1381.
(3) Kiener, D. and Minor, A. M. *Nano Lett*. **2011**, *11*, 3816–3820.
(4) Zhang, H.; Schuster, B. E.; Wei, Q.; and Ramesh, K. T. *Scripta Mater*. **2006**, *54*, 181–186.
(5) Gu, X. W.; Loynachan, C. N.; Wu, Z.; Zhang, Y. W.; Srolovitz, D. J.; and Greer, J. R. *Nano Lett*. **2012**, *12*, 6385–6392.
(6) Chen, D. Z.; Jang, D.; Guan, K. M.; An, Q.; Goddard, W. A.; and Greer, J. R. *Nano Lett*. **2013**, *13*, 4462–4468.
(7) Landau, P.; Guo, Q.; Hattar, K.; and Greer, J. R. *Adv. Funct. Mater*. **2012**, *23*, 1281–1288.